Optimization of polycaprolactone fibrous scaffold for heart valve tissue engineering

Soumen Jana[1,2,*], **Amrita Bhagia**[2], **Amir Lerman**[2]

[1]Department of Bioengineering, University of Missouri, Columbia, MO 65211, USA

[2]Division of Cardiovascular Diseases, Mayo Clinic, 200 First Street SW, Rochester, MN 55905, USA

Abstract

Pore size is generally small in nanofibrous scaffolds prepared by electrospinning polymeric solutions. Increase of scaffold thickness leads to decrease in pore size, causing impediment to cell infiltration into the scaffolds during tissue engineering. In contrast, comparatively larger pore size can be realized in microfibrous scaffolds prepared from polymeric solutions at higher concentrations. Further, microfibrous scaffolds are conducive to infiltration of reparative M2 phenotype macrophages during in vivo/in situ tissue engineering. However, rise of mechanical properties of a fibrous scaffold with the increase of polymer concentration may limit the functionality of a scaffold-based tissue-engineered heart valve. In this study, we developed microfibrous scaffolds from 14%, 16% and 18% (wt/v) polycaprolactone (PCL) polymer solutions prepared with chloroform solvent. Porcine valvular interstitial cells were cultured in the scaffolds for 14 days to investigate the effect of microfibers prepared with different PCL concentrations on the seeded cells. Further, fresh microfibrous scaffolds were implanted subcutaneously in a rat model for two months to investigate the effect of microfibers on infiltrated cells. Cell proliferation, and its morphologies, gene expression and deposition of different extracellular matrix proteins in the in vitro study were characterized. During the in vivo study, we characterized cell infiltration, and myofibroblast andM1/M2phenotypes expression of the infiltrated cells. Among different PCL concentrations, microfibrous scaffolds from 14% solution were suitable for heart valve tissue engineering for their sufficient pore size and low but adequate tensile properties, which promoted cell adhesion to and proliferation in the scaffolds, and effective gene expression and extracellular matrix deposition by the cells in vitro. They also encouraged the cells in vivo for their infiltration and effective gene expression, including M2 phenotype expression.

Keywords

*Corresponding author: Soumen Jana, sjgv7@missouri.edu.

1. Introduction

Fibrous scaffolds produced by electrospinning method have been used in tissue engineering because fibrous morphology is conducive to culturing of cells - the prime and most important component in tissue engineering [1–3]. The seeded/infiltrated cells adhere and align along the fibers of a scaffold; thus, during tissue engineering, the deposited extracellular matrix (ECM) proteins align along the fibers. If the structure of a fabricated fibrous scaffold mimics the morphology of a native tissue, tissue engineering with that fibrous scaffold has more ability to mimic morphology of the native tissue compared to that with a 3D solid porous scaffold and a hydrogel scaffold [4–6].

However, fibrous scaffolds face some problems. One is pore size in the scaffolds [6, 7]. In general, a scaffold made of nanofibers has pore size less than 10 microns (usual cell size). During tissue engineering, obstacles in cell penetration occur with the increase of nanofibrous scaffold thickness [8, 9]. Conversely, a scaffold made of microfibers shows comparatively larger pore size in general, leading to better cell penetration into the scaffold [10, 11]. Therefore in tissue engineering with requisite scaffold thickness, a microfibrous scaffold will be more efficient than a nanofibrous scaffold.

Scaffolds made of microfibers have another advantage over nanofibrous scaffolds in both in-vitro and in-vivo tissue engineering [12–15]. During in-vitro cell culturing, higher cell adhesion and spreading were observed in porous mesh, made of fibers with large diameter (in micron scale) [12]. After implantation, inflammation occurs at the implant site leading to infiltration of inflammatory Ml phenotype macrophages. At the end of inflammation cycle, reparative M2 phenotype macrophages take part in tissue generation through cellular growth and ECM deposition at the implantation site [16, 17]. Presence of microfibers in the scaffolds invokes more M2 phenotype macrophages leading to formation of thicker fibrous capsules compared to that with nanofibers in scaffolds [15].

We intend to produce microfibrous scaffold using electrospinning method for our heart valve tissue engineering project. Among various electrospinnable polymers, polycaprolactone (PCL) is easy to electrospin [18–20]. Further, biodegradation of PCL, in vitro or in vivo, does not produce any toxic byproduct, so, biomedical devices made of PCL do not face difficulties for FDA approval [20]. Biodegradation of PCL relates to its molecular weight, so, biomedical devices made of PCL will have varied in vivo shelf-life [20, 21]. Thus, we plan to use PCL microfibrous scaffolds in our future heart valve tissue engineering work.

Heart valve tissue engineering can be done in vitro, in vivo (subcutaneous) and in situ [22–24]. After heart valve replacement with an in vitro or in vivo generated tissue-engineered valve or a fresh scaffold valve, remodeling will occur in the tissue-engineered valve and tissue engineering will occur in the implanted scaffold valve. In all cases, in situ cells will penetrate into the structure and will behave according to the morphology and properties of the structure. The residing cells in native valve leaflets, the valvular interstitial cells (VICs), play a crucial role in determining the fate of the leaflets depending on the characteristics of the surrounding environment including structure and mechanical/biochemical properties of the leaflets [22–24]. Higher mechanical properties of a leaflet structure may cause the

myofibroblast phenotype expression of VICs that may directly/indirectly involve the cells in producing fibrous collagen, i.e., further hardening of the structure [18, 25, 26]. This hardening will reduce the elastomeric property of the leaflet structure required for its smooth functioning and can cause heart valve diseases.

PCL and PCL-based fibrous scaffolds have been used in heart valve tissue engineering and fiber diameters in those scaffolds are in nanoscale and/or microscale [23, 25]. We previously stated that microfibers are preferable to nanofibers for in vivo or in situ tissue engineering, especially heart valve tissue engineering; however, no reports indicate to what extent PCL microfibers will play a positive role in heart valve tissue engineering as increase in fiber diameter increases the mechanical properties of the scaffold, which adversely influences the functionality of a developing tissue heart valve, especially its leaflets. Thus, our goal is to find a PCL microfibrous scaffold with lowest allowable mechanical properties for heart valve tissue engineering.

Previous studies show that chloroform was applied as a solvent to prepare PCL solution for electrospinning PCL fibers with a diameter in the range of 3 – 5 μm [27, 28]. In our lab, we tried electrospinning of PCL (MW=80,000) at different concentrations to produce microfibers with a diameter close to 5 μm. Diameter of produced PCL fibers at the concentration of 12% (wt/v) and below was not uniform: we observed presence of nanofibers and microfibers. At 14%, diameter of the electrospun fibers was uniform and in micron scale. We thus chose three concentrations – 14%, 16% and 18% (wt/v) to prepare microfibrous scaffolds and characterize their pore sizes, fiber diameters and tensile properties. We did not choose much higher PCL concentration PCL concentration (such as 22% and upwards) as mechanical properties of fibrous scaffolds produced from high PCL concentrations could be very high, which may affect heart valve tissue engineering [25]. To find the best scaffold among all three types of microfibrous scaffolds produced from 14%, 16% and 18% (wt/v) PCL for heart valve tissue engineering, porcine valvular interstitial cells (PVICs) were cultured on those scaffolds for 14 days. Cell proliferation, its gene expression and deposition of different ECM proteins including collagen, glycosaminoglycans and elastin were assayed. Further, these three types of scaffolds were implanted for two months in a rat model subcutaneously for in vivo tissue engineering. Infiltration of cells, and their myofibroblast and M1/M2 phenotype expression were characterized to find whether in vivo outcomes can validate in vitro results.

2. Materials and methods

2.1. Nanofibrous scaffold fabrication

14%, 16% and 18% (wt/v) polycaprolactone (PCL, MW: 80 KD, Sigma Aldrich, USA) solutions in chloroform (Sigma Aldrich, USA) were electrospun on a metal plate collector to prepare three types of microfibrous scaffolds. Electro pinning parameters were: voltage - 8kV, flow rate - 0.5 ml/hr and distance between the spinneret and the collector - 15 cm. The thickness of the scaffolds was measured using a thickness measurement gauge (Mitutoyo, Japan).

2.2. SEM imaging

Dry scaffold samples were sputter coated with gold-palladium at 18 mA for 15 seconds for imaging with a scanning electron microscope (SEM) (Hitachi, Japan). Using their SEM images, morphology, fiber diameter and pore size of scaffolds were analyzed. Fiber diameters at different areas (n=10) of the SEM images (n=3 for each type) were measured using MetaMorph software (Molecular Devices, USA). Means and standard deviations of obtained data were calculated to find the fiber diameters of different types of scaffolds. Pore size was calculated from the SEM images (n=7 for each type) using ImageJ software (NIH, USA) in terms of their histogram charts which were then used to calculate their means and standard deviations.

Wet cell-cultured samples were fixed in 10% formalin for 24 hr and then were dried using critical point drying (CPD) method. Dried samples were then processed as before for SEM imaging and imaged with the SEM (Hitachi, Japan).

2.3. Tensile test

Tensile tests on scaffold samples were performed in a tensile tester (Instron, USA). Details of sample preparation and tensile testing can be found in our previous published papers [25, 29]. In brief, for each tensile test sample preparation, two hard paper window-frames with window dimensions of 10 mm × 7 mm were made. A rectangular-shaped test sample with dimensions of 14 mm × 4 mm was cut from a large fibrous scaffold and was then sandwiched and glued (Loctite super glue) between two window-frames to make a tensile test sample. The test sample was placed between the grips of a tensile tester, vertical sides of the window frames were snapped and the sample was loaded at a rate of 0.1 mm/second. The data from tensile tests (n=5 for each type of scaffold) were recorded and were used to calculate mean tensile modulus and strength for each type of scaffold and their standard deviations.

2.4. Cell seeding, culture and proliferation

Circular-shaped scaffold samples that fit to a well of a 24-well plate were cut from a large fibrous scaffold and were used for cell proliferation study. The samples were degassed overnight to remove any toxic solvent from the samples, sterilized in an ethylene oxide gas chamber and then soaked with sterile PBS in a sterile container. 1 million porcine valvular interstitial cells (PVICs) in 1 ml culture media (DMEM, 10% FBS and 1% antibiotic/antimycotic) were seeded onto each circular-shaped scaffold sample placed in a well of a 24-well plate.

Several samples of each type of scaffold were used for cell culture. After first day of culture for cell-adhesion, the seeded scaffolds were transferred to the wells of new 24-well plates in order to discard the unattached cells. The seeded cells on the scaffolds were cultured in media for 14 days with replenishing of media every three days.

Three samples of each type of scaffold were used for proliferation test. Alamar Blue (Thermo Fisher Scientific, USA) assay was performed on them at 1-, 4- and 7-day time points for the test following the company protocol. Absorbance data of assay solutions were

collected through a spectrophotometer (SpectraMax Plus 384, Molecular Devices, USA). Form the obtained data, percentages of Alamar Blue reductions were calculated following the company protocol and compared.

2.5. Implantation and explantation

Rats (Sprague Dawley, 1–2 months, ~250 gm) were used for in-vivo tissue engineering. A total of four rats (n=4) were used for this study and a total of three scaffold samples—one scaffold sample of each type (14%, 16% and 18%) were implanted in each rat. The samples were vacuum degassed overnight to remove any toxic solvent from the samples and then sterilized in ethylene oxide gas. Blood was collected from the tail vain to soak the samples before their implantations. A 4 cm incision at the dorsal region of a rat was made and the skin was loosened from the muscle to create a pocket to implant three scaffold samples sufficiently away from each other. Each scaffold sample was sutured at its four corners with a Polypropylene 5–0 suture to prohibit its displacement. After 2 months, the samples were gently explanted for their assessments. This study was performed in accordance with authorization and guidelines of the Ethical Committee of Mayo Clinic, Rochester, MN, USA.

2.6. Staining

Wet cell-cultured samples were fixed in 4% methanol-free formaldehyde (Thermo Fisher Scientific, USA) overnight at 4°C. Applying paraffinization process, samples were paraffinized. 5 micron thick sections were cut from the paraffinized samples for staining.

The sections were stained separately with hematoxylin and eosin (Thermo Fisher Scientific, USA), picrosirius red (ScyTek Lab, USA) and Safranin O (ScienCell Research Lab, USA) for their histological analysis following manufacturer protocols and/or our previously defined protocols [18, 29].

The sections were stained separately with elastin (ab21610, abeam, USA), tropoelastin (ab21600, abeam, USA), vimentin (ab92547, abeam, USA) and α=smooth muscle actin (SMA) markers for their immunohistochemical analysis following manufacturer protocols and/or our previously defined protocols [18, 29].

Following the procedures stated above, explanted samples were fixed, paraffinized, sectioned and stained separately with DAPI (Thermo Fisher Scientific, USA) for their immunofluorescent analysis [18, 25, 30].

2.7. Gene expression

Fresh cell-cultured samples and explanted samples were collected. Applying RNeasy mini kit from Qiagen, Germany, RNAs from the cells in the samples were extracted. The RNAs were then purified with DNase I from Life technologies, USA. Applying High-Capacity cDNA Reverse Transcription kit with RNase Inhibitor from Applied Biosystems, USA, purified RNAs were converted to first-strand cDNAs. Applying Lightcycler 480 Probe master mix from Roche, USA, the produced cDNA transcripts were then probed with TaqMan assays for vimentin (Ss04330801_gH), and α-smooth muscle actin (α-SMA,

Ss04245588_ml) on in vitro samples, for vimentin (Rn00579738_ml), α-SMA (Rn01759925_g1), INOS (Rn06325074_m1) and CD-163 (Rn01492530_ml) on in vivo samples. In all steps, protocols supplied by manufacturers were used to obtain gene expression data. Obtained target gene data were normalized against ACTB level and analyzed using the comparative cycle threshold (Ct) method.

2.8. Image Quantification

MetaMorph software (Molecular Devices Inc., USA) was used to quantify the signal in the images obtained from histology-stained and immunostained samples. Percentage of area covered by any specific signal in a stained image with respect to total area of that image was used as quantified data for that signal. Sufficient number of samples (n=10) was used for each type of scaffold for a particular signal to obtain data that were used to calculate the mean and standard deviation.

ImageJ software (NIH, USA) was used to create intensity profile across the H&E-stained cross-sectional images of PVIC-cultured scaffolds in transverse direction.

2.9. Statistical analysis

Mean ± standard deviation (SD) was used to report data. An unpaired t-test for two-group comparisons and a one-way ANOVA with Tukey's post-hoc test for three-group comparisons were conducted. P values <0.05 were applied to indicate significance.

3. Results

3.1. Fibrous scaffold fabrication

14%, 16% and 18% polycaprolactone solutions in chloroform were electrospun with specific electrospinning parameters (flow rate: 0.5ml/hr, voltage: 8kV and spinneret-collector distance: 15 cm) to produce fibrous scaffolds containing microfibers only. Thicknesses of the produced scaffolds were in the range of 200 – 300 μm. Scanning electron microscopic (SEM) images of the scaffolds were obtained to observe their morphologies (Figure 1). In all types of scaffolds (14%, 16% and 18%), fibers were evenly distributed and perfectly cylindrical. It was also observed that fibers were separate from each other (did not coalesce). At higher magnification it was clear.

Using ImageJ software, pore size in each type of scaffold was assayed (Figure 2). Pore size in 14% scaffold (20.19 ± 7.36 μm) was significantly lower than that in both 16% (27.46 ± 11.58 μm) and 18% scaffold (27.14 ± 12.14 μm). Pore size in 16% scaffold was higher than that in 18% scaffold but was not significantly high. SEM images of fibrous scaffolds at higher magnification in Figure 1 show the differences in their pore sizes.

Fiber diameter in each type of scaffold was measured using MetaMorph software (Figure 2). Fiber diameter in 14% scaffold (4.50 ± 0.53 μm) was significantly lower than that in 16% scaffold (6.00 ± 0.40 μm) and fiber diameter in 16% scaffold (6.00 ± 0.40 μm) was significantly lower than that in 18% scaffold (6.86 ± 0.37 μm). SEM images of different fibrous scaffolds at higher magnification in Figure 1 distinctly show the differences in their fiber diameters.

3.2. Tensile test

Tensile tests on different types of scaffolds (14%, 16% and 18%) were performed in a tensile tester. Figure 3a shows the typical tensile curves of different types of scaffolds. Apparently, it can be observed that 16% scaffold was stronger than 14% and 18% scaffold was stronger than 16%. Then, recorded data from the tensile tests of different types of scaffolds were analysed to find their tensile moduli and strengths (Figure 3b). Tensile moduli of both 16% and 18 % scaffolds (7.88 ± 1.10 MPa and 8.91 ± 0.40 MPa, respectively) were significantly higher than that of 14% scaffold (3.41 ± 0.40 MPa). Similarly, tensile strengths of 16% and 18 % scaffolds (0.99 ± 0.16 MPa and 1.26 ± 0.18 MPa, respectively) were significantly higher than that of 14% scaffold (0.59 ± 0.05 MPa). However, both tensile modulus and strength of 18% scaffold were not significantly higher than that of 16% scaffold.

3.3. Cell proliferation

Circular-shaped samples were cut from different types of scaffolds (Figure 4a) and 1 million PVICs were cultured on the circular surface of each of them for a total of 7 days for a cell proliferation study. Cells were counted after 1-, 3- and 7-day periods of culture to verify the proliferation of PVICs on 14%, 16% and 18% scaffolds (Figure 4b) in terms of Alamar Blue reduction. The higher the reduction, the higher the cell number presents on a scaffold. After the first day of culture, cell number was highest on 14% scaffold (39.48 ± 0.51) and lowest on 18% scaffold (34.21 ± 0.96) which meant that cell adherence was best on 14% scaffold and worst on 18% scaffold. Number of cells on 16% scaffold (35.63 ± 2.21) was not significantly higher than that on 18% scaffold (34.21 ± 0.96) at day 1. A close to similar trend was seen at day 4, except the number of cells on 18% scaffold (37.92 ± 1.47) was bit higher (not significant) than that on 16% scaffold (37.49 ± 0.69). Number of cells on 14% scaffold (40.95 ± 0.82) was significantly higher than that on both 16% (37.49 ± 0.69) and 18% (37.92 ± 1.47) scaffolds at day 4. At day 7, lowest to highest cell number was in this order: 16% scaffold (41.35 ± 1.28), 14% scaffold (41.70 ± 2.11) and 18% scaffold (42.72 ± 0.93) but they were not significantly different. After 7 days culture, After 7 d culture, proliferation of cells was lowest on 14% scaffold (5.63%), and highest on 18% scaffold (24.88%), while proliferation on 16% scaffolds (16.02%) was in between.

3.4. Cell morphology and cell penetration

PVICs were cultured on different types of scaffolds (14%, 16% and 18%) for 14 days. To observe cell morphology on the circular surfaces of the scaffolds, cell-cultured samples were processed and imaged with scanning electron microscopy (SEM) (Figure 5a). Cells on the 14% scaffold had an oval shape whereas they were flat on 16% scaffold. Flatness of the cells was greater on 18% scaffold. Due to the oval shape of cells on 14% scaffold, the area of spreading of each cell was less compared to that on 16% and 18% scaffolds. Spreading of each cell was greatest on 18% scaffold.

To confirm cell penetration into the scaffolds, cross-sections (transverse to circular surface) of 14-day-cultured samples were stained with hematoxylin and eosin and imaged with a light microscope (Nikon, Japan) (Figure 5b). Presence of cells inside each type of scaffold was observed. During cell seeding, cells penetrated into the scaffolds, and then proliferated with passage of time. The PVICs in each scaffold can be seen distinctly in the image at

higher magnification (Figure 5c). Each image in figure 5c relates to the square section in the corresponding image in figure 5b. However, this square section is only part of the whole image; thus, ImageJ software was used to create an intensity profile across each image strip in transverse direction (Supplementary section, Figure S1). The intensity profile is quite horizontal along the strip i.e., PVICs were present throughout each scaffold.

A cellular layer (pointed by a black arrow) formed on the circular surface of each type of scaffold after 14 days cell culture. On the surface of 14% scaffold, the cellular layer was thicker (visually) compared to that on the surfaces of 16% and 18% scaffolds. The thinnest cellular layer was observed on the surface of 18% scaffold. This observation confirmed the oval shape of PVICs on 14% scaffold and comparatively flat shape on 16% and 18% scaffolds that were seen in their SEM images (Figure 5a).

3.5. Gene expression

Gene expression assay was performed on the cells from 14-day cell-cultured samples. PVICs are fibroblast-like cells that show quiescent fibroblast phenotype in a healthy valve leaflet and quiescent or active myofibroblast phenotype in growing state, remodeling state or damaged state of a valve leaflet depending on degree of any state. Vimentin marker (of fibroblast cell) along with alpha-smooth muscle actin (α-SMA) marker (of smooth muscle cell) represent a marker for myofibroblast phenotype of PVICs.

The vimentin expression of the PVICs from 18% and 14% scaffolds were highest and lowest, respectively and they were significantly different (Figure 6a). This expression from 16% scaffold was in between. Similarly, the α-SMA expression of the PVICs from 18% and 14% scaffolds were highest and lowest, respectively and they were significantly different. The α-SMA expression of the PVICs from 16% scaffold was in between the expression from 14% and 18% scaffolds.

To see the presence of vimentin and α-SMA protein markers in PVICs, different types of cell-cultured scaffolds were stained cross-sectionally with those markers and imaged with a light microscope (Nikon, Japan) (Figure 6b). The PVICs in all types of cell-cultured samples showed presence of vimentin and α-SMA protein markers.

3.6. Extracellular matrix assay

In tissue engineering, deposition of various extracellular matrices including collagen, glycosaminoglycans and elastin is important to achieve the desired functionalities. Staining method was applied to see their presence in the PVIC-cultured scaffolds. For collagen detection, PVIC-cultured scaffolds were stained cross-sectionally with picrosirius-red stain and imaged with bright-field light (Figure 7a). To confirm their presence, SEM images of PVIC-cultured scaffolds were taken cross-sectionally at high magnification. In all three scaffold systems, collagen fibrils were present (Figure 7b). Visually, both in stained and SEM images, density of deposited collagen in 18% scaffold was lower than that in the two other types of scaffolds. To confirm it, image-based collagen quantification was performed on picrosirius-red stained images (Figure 7c). Amount of collagen was highest on 14% scaffold (12.41 ±1.3) and lowest on 18% scaffold (5.58± 0.95); they differed significantly. Also amount of collagen on 14% scaffold (12.41 ± 1.3) was significantly higher than that on

16% scaffold (10.09 ± 1.22) which was higher than the amount of collagen on 18% scaffold (5.58 ± 0.95).

Glycosaminoglycans (GAG) in the PVIC-cultured scaffolds were stained cross-sectionally with Safranin O stain (Figure 8a). All scaffolds showed the presence of GAG after 14 days culturing of PVICs. The amount of GAG found through image-based quantification measurement was highest on the 16% scaffold (3.10 ± 0.97) and lowest on 18% scaffold (2.33 ± 0.73); however, their difference was not significant. Amount of GAG on 14% scaffold (3.00 ± 0.35) was significantly higher than that on 18% scaffold (2.33 ± 0.73) (Figure 8d).

To detect presence of tropoelastin and elastin in the cultured scaffolds, the samples were immunostained cross-sectionally with their respective markers (Figure 8b–c). Presence of both tropoelastin and elastin in cultured scaffolds were observed. Tropoelastin is a precursor of elastin in matrix development. By applying MetaMorph software, their quantities were assessed (Figure 8d). Amount of tropoelastin in 14% scaffold (10.80 ± 1.20) was significantly higher than that in both 16% (8.74 ± 0.65) and 18% (6.49 ± 1.87) scaffolds. Similarly, amount of tropoelastin in 16% scaffold was significantly higher than that in 18% scaffold. Among all three types of scaffolds, elastin deposition was highest on 16% scaffold (2.93 ± 0.59) and was lowest on 14% scaffold (2.65 ± 0.53). On 18% scaffold, elastin deposition (2.75 ± 0.76) was in between.

3.7. In vivo study

3.7.1. Cell infiltration—14%, 16% and 18% microfibrous scaffolds were implanted subcutaneously for two months in a rat model for in vivo tissue engineering assays (Supplementary section, Figure S2). Explanted samples were stained cross-sectionally with DAPI to find the infiltrated cells. Cells were observed in all explanted samples (Figure 9a). Visually, more cells were observed in 14% scaffold compared to that in 16% and 18% scaffolds. In 14% scaffold, cells were infiltrated deep inside the scaffold whereas in 16% and 18% scaffolds, more cells were on the scaffolds' circular surfaces (shown by white arrows) that were attached to the skins of rats during implantation. To compare number of cells in those scaffolds accurately, MetaMorph software was applied to assess their numbers (Figure 9b). Number of cells in 14% (1 ± 0.10) scaffold was significantly higher than that in both 16% (0.78 ± 0.13) and 18% (0.73 ± 0.12) scaffolds and number of cells in 16% (0.78 ± 0.13) and 18% (0.73 ± 0.12) scaffolds did not differ significantly.

3.7.2. Gene expression—Vimentin expression of infiltrated cells in 14%, 16% and 18% scaffolds were not significantly different (Figure 10a). This gene expression of infiltrated cells was quite similar to that of in vitro-cultured PVICs. Conversely, α-SMA expression of infiltrated cells in 14% scaffold was significantly lower than that of infiltrated cells in both 16% and 18% scaffolds. However, α-SMA expression of these cells in 16% scaffold and 18% scaffold were not significantly different. Interestingly, α-SMA expression of infiltrated cells in different scaffold systems was quite similar to that of in vitro-cultured PVICs.

It is reported that microfibers invoke more M2 phenotype macrophages than do M1 phenotype macrophages [15]. To find the efficacy of 14%, 16% and 18% microfibrous scaffolds on invoking M2 phenotype macrophages, Ml and M2 gene expression assays on infiltrated cells were performed. M2 phenotype expression of the infiltrated macrophages wassignificantly higher than Ml phenotype expression of those infiltrated macrophages in all three 14%, 16% and 18% scaffolds (Figure 10b).

4. Discussion

Tissue engineering approach is a prudent solution to current problematic prosthetic heart valves that are applied to mitigate heart valve diseases [24, 31, 32]. In the scaffold-based tissue engineering method, a scaffold in which cells can reside needs to be favorable for sufficient cell penetration/infiltration, cell proliferation and ECM deposition, etc. [33–35]. For sufficient cell penetration/infiltration, pore size of a scaffold should be more than the cell size generally 10 μm [6, 27].

Among different types of scaffolds, fibrous scaffolds are unique for the superior cell adhesion to the fibers in a scaffold and cell orientation along the fibers [35–37]. Fibrous scaffolds applied for tissue engineering are usually produced by electrospinning method and fibers both in nanoscale and microscale can be produced with this method by varying the concentration of polymer solution and electrospinning parameters including voltage, flow rate of solution and distance between a spinneret and a collector [27, 35]. One disadvantage with nanofibrous scaffolds is that with the increased thickness, pore size in the scaffolds decreases leading to prohibition of cell penetration/infiltration into the scaffolds during tissue engineering [8, 9]. Conversely, microfibrous scaffolds show sufficient pore size for cell penetration/infiltration throughout the scaffolds; with increase of polymer concentration in an electrospinning polymer solution, pore size generally increases which is favorable for improved cell penetration/infiltration [10, 11]. Further, microfibers showed some specific advantages over nanofibers in tissue engineering including better cell adhesion and spreading. However, increase of polymer concentration augments the mechanical properties of microfibrous scaffolds, and those with high mechanical properties may not be useful for heart valve tissue engineering. This especially applies for leaflet tissue engineering as the VICs in a tissue-engineered leaflet may show unwanted myofibroblast phenotype [26, 38]. This study aims to find an optimal polycaprolactone (PCL) concentration to develop a microfibrous scaffold for efficient heart valve tissue engineering.

It is observed that chloroform-based PCL solution was used to produce microfibers in an electrospinning setup [27, 28]. In our preliminary study, microfibers were produced from PCL (MW=80,000) at its lowest concentration of 14% (wt/v) in chloroform; fiber diameter was close to 5 μm. Therefore, PCL with concentrations of 14% (wt/v) and above (16% and 18%) in chloroform were applied to produce electrospun scaffolds consisting of only microfibers. Those microfibrous scaffolds were produced with specific electrospining parameters - flow rate: 0.5ml/hr, voltage: 8kV and spinneret-collector distance: 15 cm. If the parameters were changed a bit - for example, flow rate: 1ml/hr and voltage: 10kV, presence of nanofibers along with microfibers in the scaffolds were observed (Supplementary section, Figure S3). Higher flow rate and voltage caused the formation of two Taylor cones at the tip

of the spinneret—the larger Taylor cone produced microfibers while the smaller one produced nanofibers [39]. Another reason was that higher amount of solution jet was liable to split during whipping in air leading to formation of both nanofibers and microfibers. High voltage would create high repulsion force among the similarly charged molecules in the Taylor cone-shaped solution at the needle tip and higher electrostatic force between the solution at the needle tip and the collector. Both would work against the surface tension of the solution at the tip and the solution would split causing the generation of nanofibers and microfibers. However, with increase of PCL concentration, nanofibers decreased in number. Viscosity of PCL solutions increases with PCL concentration i.e. high PCL concentration creates high viscoelastic forces which resists splitting of charged solution jet during whipping leading to less number of nanofibers in the scaffold [40].

The produced microfibrous scaffolds were characterized physically and biologically for their usefulness in heart valve tissue engineering. With the increase of PCL concentration, both fiber diameter and pore size in the respective scaffolds increased. Increase of PCL concentration increases the viscoelastic forces of the solution, which decreases splitting of the charge solution during whipping, resulting in increase of fiber diameter [40]. Further, with the increase of fiber diameter, average pore size in the electrospun scaffolds increases [19, 41]. High pore size will certainly improve cell penetration/infiltration during tissue engineering leading to improved tissue formation.

Residing VICs in native leaflets are sensitive to the mechanical properties of their surrounding structures, and phenotype of VICs changes with the variation of the mechanical properties [26, 38]. VICs show quiescent fibroblast phenotype in mature healthy leaflets and quiescent to active myofibroblast phenotype during their remodeling, growth and diseases depending on the degree of their states [38, 42]. They also show active myofibroblast phenotype on scaffolds with high mechanical stiffness [25]. Active myofibroblast phenotype in PVICs caused by any abnormal (diseases and damage) and/or external (mechanical stiffness), may result in production of fibrotic ECM, which reduces the functional efficiency of the remodeled or engineered tissues [43]. Tensile properties of scaffolds increased with the increase of polymer concentration in the scaffolds. Although no scaffold structure would exist at the end; during tissue engineering the mechanical properties of the fibrous scaffold would influence the phenotype of seeded/infiltrated PVICs. Among 14%, 15% and 18% microfibrous scaffolds, tensile stiffness was lowest in 14% scaffold. Considering the adversary of high tensile stiffness of a scaffold on PVICs, 14% scaffold may be more appropriate than others in heart valve tissue engineering. Tensile modulus of 14% scaffold was ~3.41 MPa and previous studies show that tissue engineered valves with a tensile modulus of 3.49 MPa were successfully tested in heart valve application in an animal model [44, 45]. Thus, a microfibrous heart valve scaffold produced with 14% PCL is expected to bear the physiological pressure upon heart valve replacement with the microfibrous scaffold.

Adhesion of PVICs was highest on 14% scaffold and comparatively less on 16% and 18% scaffolds. Higher tensile properties of 16% and 18% scaffolds compared to 14% were the reason for less cell adhesion [46]. Although adhesion of PVICs to softer 14% scaffold was higher compared to other stronger scaffolds (16% and 18%), less proliferation of the cells occurred in 14% scaffold compared to that in other scaffolds; however, the differences in cell

proliferation in those scaffolds were not significant. Considering this proliferation outcome, 14% scaffold may take more time for tissue growth compared to other scaffolds; yet, 14% scaffold would have less adverse influence on the cells in producing fibrotic ECM during tissue engineering due to its lower mechanical properties [26, 47].

Like previously reported studies, PVICs on the microfibrous scaffolds with lowest tensile modulus i.e. on 14% scaffold showed oval shape; on scaffolds with comparatively higher tensile modulus i.e. on 16% and 18% scaffolds, PVICs showed comparatively flat cell shape [37, 47, 48]. When cells come in contact with scaffolds, their adhesion, shape, proliferation and differentiation are influenced by several factors including composition, morphology and mechanical properties such as stiffness/strength of the scaffolds [49, 50]. Due to sufficient pore size in the scaffolds, seeded PVICs penetrated into the scaffolds and grew over time. PVICs in 14% scaffold showed less expression of both vimentin and α-smooth muscle actin (α-SMA) compared to that in 16% and 18% scaffolds. Thus, although PVICs showed myofibroblast phenotype in all types of scaffolds, the cells were less active in 14% scaffold than in 16% and 18% scaffolds. Highly active myofibroblast phenotype expression of PVICs may cause deposition of fibrotic collagen and the generated tissue, consisting of fibrotic collagen, may not achieve required functionalities [51]. Further, fibrotic collagen in a tissue-engineered heart valve may cause calcification leading to stenosis and regurgitation in the heart valve [43, 52].

Deposition of collagen fibrils by PVICs in the scaffolds was characterized by picrosirius red staining and collagen fibrils were found in all of them. Their SEM images distinctly confirmed the presence of collagen fibrils in all scaffolds. The collagen contents in the scaffolds were quantified by applying a software-based method on their stained images instead of applying a calorimetric method on their PVIC-cultured samples [53]. The reason is that during protein quantification, the scaffold material (PCL) melted i.e. pores were sealed while heating the samples in respective liquid chemicals and the melted PCL barred the release of proteins from the scaffolds into the chemicals. In 14% scaffold, collagen deposition was significantly higher than that in both 16% and 18% scaffolds. Further, in 16% scaffold, collagen deposition was significantly higher than that in 18% scaffold. These results suggest that lower mechanical properties of the 14% scaffold compared to that of other scaffolds may provide an appropriate environment for the cell growth and heart valve tissue engineering.

Beside collagen, deposition of glycosaminoglycans (GAG), tropoelastin and elastin by PVICs in the scaffolds were characterized qualitatively by staining. For the same reason stated before, their quantitative characterizations were assayed by applying a software-based method on their stained images instead of applying a calorimetric method on their PVIC-cultured samples [53]. In all scaffolds, deposition of GAG was observed and GAG in 14% scaffold was significantly higher than in 18% scaffold. Presence of tropoelastin - a precursor of elastin was observed in all scaffolds. As with collagen, in 14% scaffold, tropoelastin deposition was significantly higher than that in both 16% and 18% scaffolds. On the other hand, similar to GAG, elastin deposition in 14% scaffold was significantly higher than that in 18% scaffold. Considering the above protein deposition results, it can be said that deposition of ECM materials in 14% scaffold was significantly higher than that in other

scaffolds. Heart valve leaflets consist of different ECM proteins including collagen, GAG and elastin and in 14% scaffold, we saw the highest deposition of these ECM proteins. Thus, among all the scaffold types, 14% scaffold may provide a comparatively better environment for functional heart valve tissue construct development.

To scrutinize the positive in vitro results, we performed in vivo tissue engineering in 14%, 16% and 18% scaffolds by implanting them for two months in a rat model subcutaneously in its dorsal area. Comparatively, the softer 14% scaffold had more cell infiltration. Further, the cells in this 14% scaffold infiltrated deep inside the scaffold, while in 16% and 18% scaffolds, most cells were near their surfaces. Despite higher pore sizes in 16% and 18% scaffolds, fewer cells infiltrated inside the 16% and 18% scaffolds, which suggest that higher mechanical properties of 16% and 18% scaffolds compared to that of 14% scaffold possibly prohibited cell infiltration.

Higher vimentin and α-SMA expression of the infiltrated cells were observed in 16% and 18% scaffolds than in 14% scaffold. There were differences in fiber diameter, pore size and mechanical properties of the scaffolds, and mechanical properties could be the main influence in determining the cellular characteristics. Thus, increase in mechanical properties of scaffolds raised myofibroblast phenotype expression of the infiltrated cells, which may provoke production of fibrous collagen leading to hardening of developing tissues, a phenomenon detrimental to heart valve tissue engineering [26, 54]. In this respect, 14% scaffold would have positive influence in terms of lower myofibroblast expression of the residing cells during heart valve tissue engineering. Due to microscale diameter of the fibers, more macrophages of M2 phenotype than of M1 phenotype infiltrated into the scaffolds, which confirmed our hypothesis that microfibrous scaffolds are more conducive compared to nanofibrous scaffolds for in vivo/in situ heart valve tissue engineering.

In summary, 14%, 16% and 18% scaffolds showed microfibers and sufficient pore sizes in their structures, required for sufficient cell penetration and cellularization during in-vitro or in-vivo tissue engineering. However, compared to the rest, 14% scaffold had lower tensile properties which possibly caused lower myofibroblast expression by the residing cells, higher ECM deposition by PVICs and higher M2 phenotype expression by the infiltrated macrophage in this scaffold compared to others; thus may be the best for heart valve tissue engineering. Our goal is to develop a heart valve-shaped microfibrous scaffold with three leaflets and a conduit that will be used for heart valve replacement. The heart valve scaffold will be transformed into a tissue-engineered heart valve through in situ tissue engineering.

5. Conclusion

This study sought a proper PCL concentration to produce a microfibrous scaffold with sufficient pore size for heart valve tissue engineering. Microfibrous scaffolds were produced from 14%, 16% and 18% (wt/v) PCL concentrations and PVICs were cultured in them for 14 days. With increase of PCL concentration, fiber diameter and average pore size in the respective scaffolds increased. Tensile stiffness and strength of 14 % scaffold were less than that of 16% and 18% scaffolds. Adhesion of PVICs to 14% scaffold was higher than that to other scaffolds. Proliferation of PVICs in different types of scaffolds was not significantly

different. After 14 days culture, PVICs on 14% scaffold had oval-shaped morphology and on 16% and 18% scaffolds, they had a comparatively flat-shaped morphology. Due to sufficient pore size in all types of scaffolds, PVICs penetrated into the scaffolds and grew with passage of time. PVICs in 16% and 18% scaffolds showed more active myofibroblast phenotype than in 14% scaffolds. Presence of different ECM including collagen, glycosaminoglycans and elastin was observed in all scaffolds after 14 days culture. Deposition of collagen and tropoelastin by PVICs on 14% scaffold was significantly higher than on 16% and 18% scaffolds and deposition of glycosaminoglycans on 14% scaffold was significantly higher than on 18% scaffold. Higher numbers of cell infiltration, and lower myofibroblast and higher M2 phenotype expression by the infiltrated cells in 14% scaffold compared to those in 16% and 18% scaffolds were observed in the in vivo study. Considering all these characterized data, it seems that microfibrous scaffolds made from 14% PCL could fit best for heart valve tissue engineering.

Supplementary Material

Refer to Web version on PubMed Central for supplementary material.

Acknowledgment

References

[1]. Leung M, Jana S, Tsao C-T, Zhang M. Tenogenic differentiation of human bone marrow stem cells via a combinatory effect of aligned chitosan–poly-caprolactone nanofibers and TGFβ3. Journal of Materials Chemistry B. 2013;1:6516–24. [PubMed: 32261328]

[2]. Onoe H, Takeuchi S. Cell-laden microfibers for bottom-up tissue engineering. Drug Discovery Today. 2015;20:236–46. [PubMed: 25448757]

[3]. Tseng H, Puperi DS, Kim EJ, Ayoub S, Shah JV, Cuchiara ML, et al. Anisotropic poly(ethylene glycol)/polycaprolactone hydrogel-fiber composites for heart valve tissue engineering. Tissue Eng Part A. 2014;20:2634–45. [PubMed: 24712446]

[4]. Bertassoni LE, Cecconi M, Manoharan V, Nikkhah M, Hjortnaes J, Cristino AL, et al. Hydrogel bioprinted microchannel networks for vascularization of tissue engineering constructs. Lab Chip. 2014;14:2202–11. [PubMed: 24860845]

[5]. Jana S, Leung M, Chang J, Zhang M. Effect of nano- and micro-scale topological features on alignment of muscle cells and commitment of myogenic differentiation. Biofabrication. 2014;6:035012. [PubMed: 24876344]

[6]. Loh QL, Choong C. Three-dimensional scaffolds for tissue engineering applications: role of porosity and pore size. Tissue engineering Part B, Reviews. 2013;19:485–502. [PubMed: 23672709]

[7]. Choi S-W, Zhang Y, Xia Y. Three-Dimensional Scaffolds for Tissue Engineering: The Importance of Uniformity in Pore Size and Structure. Langmuir. 2010;26:19001–6. [PubMed: 21090781]

[8]. Chandrasekaran AR, Venugopal J, Sundarrajan S, Ramakrishna S. Fabrication of a nanofibrous scaffold with improved bioactivity for culture of human dermal fibroblasts for skin regeneration. Biomed Mater. 2011;6:015001. [PubMed: 21205999]

[9]. Zhong S, Zhang Y, Lim CT. Fabrication of large pores in electrospun nanofibrous scaffolds for cellular infiltration: a review. Tissue engineering Part B, Reviews. 2012;18:77–87. [PubMed: 21902623]

[10]. Bagherzadeh R, Latifi M, Kong L. Three-dimensional pore structure analysis of polycaprolactone nano-microfibrous scaffolds using theoretical and experimental approaches. J Biomed Mater Res A. 2014;102:903–10. [PubMed: 23554325]

[11]. Simonet M, Stingelin N, Wismans JGF, Oomens CWJ, Driessen-Mol A, Baaijens FPT. Tailoring the void space and mechanical properties in electrospun scaffolds towards physiological ranges. Journal of Materials Chemistry B. 2014;2:305–13. [PubMed: 32261509]

[12]. Bernatchez SF, Parks PJ, Gibbons DF. Interaction of macrophages with fibrous materials in vitro. Biomaterials. 1996;17:2077–86. [PubMed: 8902241]

[13]. McWhorter FY, Wang T, Nguyen P, Chung T, Liu WF. Modulation of macrophage phenotype by cell shape. Proceedings of the National Academy of Sciences. 2013;110:17253.

[14]. Chen S, Jones JA, Xu Y, Low HY, Anderson JM, Leong KW. Characterization of topographical effects on macrophage behavior in a foreign body response model. Biomaterials. 2010;31:3479–91. [PubMed: 20138663]

[15]. Sanders JE, Bale SD, Neumann T. Tissue response to microfibers of different polymers: polyester, polyethylene, polylactic acid, and polyurethane. J Biomed Mater Res. 2002;62:222–7. [PubMed: 12209942]

[16]. Jablonski KA, Amici SA, Webb LM, Ruiz-Rosado Jde D, Popovich PG, Partida-Sanchez S, et al. Novel Markers to Delineate Murine Ml and M2 Macrophages. PLoS One. 2015;10:e0145342. [PubMed: 26699615]

[17]. Mills CD. M1 and M2 Macrophages: Oracles of Health and Disease. Critical reviews in immunology. 2012;32:463–88. [PubMed: 23428224]

[18]. Jana S, Lerman A, Simari RD. In Vitro Model of a Fibrosa Layer of a Heart Valve. ACS Appl Mater Interfaces. 2015;7:20012–20. [PubMed: 26295833]

[19]. Kievit FM, Cooper A, Jana S, Leung MC, Wang K, Edmondson D, et al. Aligned chitosanpolycaprolactone polyblend nanofibers promote the migration of glioblastoma cells. Advanced Healthcare Materials. 2013;2:1651–9. [PubMed: 23776187]

[20]. Woodruff MA, Hutmacher DW. The return of a forgotten polymer—Polycaprolactone in the 21st century. Progress in Polymer Science. 2010;35:1217–56.

[21]. Leung M, Cooper A, Jana S, Tsao CT, Petrie TA, Zhang M. Nano fiber-based in vitro system for high myogenic differentiation of human embryonic stem cells. Biomacromolecules. 2013;14:4207–16. [PubMed: 24131307]

[22]. Bennink G, Torii S, Brugmans M, Cox M, Svanidze O, Ladich E, et al. A novel restorative pulmonary valved conduit in a chronic sheep model: Mid-term hemodynamic function and histologic assessment. J Thorac Cardiovasc Surg. 2018;155:2591–601 e3. [PubMed: 29366582]

[23]. Masoumi N, Annabi N, Assmann A, Larson BL, Hjortnaes J, Alemdar N, et al. Tri-layered elastomeric scaffolds for engineering heart valve leaflets. Biomaterials. 2014;35:7774–85. [PubMed: 24947233]

[24]. Nakayama Y, Takewa Y, Sumikura H, Yamanami M, Matsui Y, Oie T, et al. In-body tissueengineered aortic valve (Biovalve type VII) architecture based on 3D printer molding. J Biomed Mater Res B Appl Biomater. 2015;103:1–11. [PubMed: 24764308]

[25]. Jana S, Lerman A. Behavior of valvular interstitial cells on trilayered nanofibrous substrate mimicking morphologies of heart valve leaflet. Acta Biomater. 2019;85:142–56. [PubMed: 30528607]

[26]. Wang H, Tibbitt MW, Langer SJ, Leinwand LA, Anseth KS. Hydrogels preserve native phenotypes of valvular fibroblasts through an elasticity-regulated PI3K/AKT pathway. Proc Natl Acad Sci U S A. 2013;110:19336–41. [PubMed: 24218588]

[27]. Lowery JL, Datta N, Rutledge GC. Effect of fiber diameter, pore size and seeding method on growth of human dermal fibroblasts in electrospun poly(epsilon-caprolactone) fibrous mats. Biomaterials. 2010;31:491–504. [PubMed: 19822363]

[28]. Del Gaudio C, Bianco A, Grigioni M. Electrospun bioresorbable trileaflet heart valve prosthesis for tissue engineering: in vitro functional assessment of a pulmonary cardiac valve design. Annali dell'Istituto superiore di sanita. 2008;44:178–86.

[29]. Jana S, Lerman A. Effect of an underlying substrate in a nanofibrous membrane system on cultured cells. Biomedical Physics & Engineering Express. 2016;2:045001(1–13).

[30]. Jana S, Hennessy R, Franchi F, Young M, Hennessy R, Lerman A. Regeneration ability of valvular interstitial cells from diseased heart valve leaflets. RSC Advances. 2016;6:113859–70.

[31]. Hobson CM, Amoroso NJ, Amini R, Ungchusri E, Hong Y, D'Amore A, et al. Fabrication of elastomeric scaffolds with curvilinear fibrous structures for heart valve leaflet engineering. J Biomed Mater Res A. 2015;103:3101–6. [PubMed: 25771748]

[32]. Jana S, Simari RD, Spoon DB, Lerman A. Drug delivery in aortic valve tissue engineering. J Control Release. 2014;196:307–23. [PubMed: 25459428]

[33]. Carletti E, Motta A, Migliaresi C. Scaffolds for tissue engineering and 3D cell culture. Methods in Molecular Biology. 2011;695:17–39. [PubMed: 21042963]

[34]. Hollister SJ. Porous scaffold design for tissue engineering. Nat Mater. 2005;4:518–24. [PubMed: 16003400]

[35]. Li W-J, Cooper JA Jr. Fibrous Scaffolds for Tissue Engineering. In: Burdick JA, Mauck RL, editors. Biomaterials for Tissue Engineering Applications: A Review of the Past and Future Trends. New York: Springer; 2011 p. 47–73.

[36]. Cooper A, Jana S, Bhattarai N, Zhang M. Aligned chitosan-based nanofibers for enhanced myogenesis. Journal of Materials Chemistry. 2010;20:8904–11.

[37]. Jana S, Levengood SKL, Zhang M. Anisotropic Materials for Skeletal-Muscle-Tissue Engineering. Advanced materials (Deerfield Beach, Fla). 2016;28:10588–612.

[38]. Wang H, Haeger SM, Kloxin AM, Leinwand LA, Anseth KS. Redirecting valvular myofibroblasts into dormant fibroblasts through light-mediated reduction in substrate modulus. PLoS One. 2012;7:e39969. [PubMed: 22808079]

[39]. Morad MR, Rajabi A, Razavi M, Sereshkeh SRP. A Very Stable High Throughput Taylor Cone-jet in Electrohydrodynamics. Scientific reports. 2016;6:38509. [PubMed: 27917956]

[40]. Nezarati RM, Eifert MB, Cosgriff-Hemandez E. Effects of humidity and solution viscosity on electrospun fiber morphology. Tissue Engineering Part C, Methods. 2013;19:810–9. [PubMed: 23469941]

[41]. Pham QP, Sharma U, Mikos AG. Electrospun poly(epsilon-caprolactone) microfiber and multilayer nano fiber/microfiber scaffolds: characterization of scaffolds and measurement of cellular infiltration. Biomacromolecules. 2006;7:2796–805. [PubMed: 17025355]

[42]. Rabkin-Aikawa E, Farber M, Aikawa M, Schoen FJ. Dynamic and reversible changes of interstitial cell phenotype during remodeling of cardiac valves. Journal of Heart Valve Disease. 2004;13:841–7. [PubMed: 15473488]

[43]. Miller JD, Weiss RM, Heistad DD. Calcific aortic valve stenosis: methods, models, and mechanisms. Circ Res. 2011;108:1392–412. [PubMed: 21617136]

[44]. Robinson PS, Johnson SL, Evans MC, Barocas VH, Tranquillo RT. Functional tissueengineered valves from cell-remodeled fibrin with commissural alignment of cell-produced collagen. Tissue Engineering Part A. 2008;14:83–95. [PubMed: 18333807]

[45]. Syedain ZH, Bradee AR, Kren S, Taylor DA, Tranquillo RT. Decellularized tissueengineered heart valve leaflets with recellularization potential. Tissue Eng Part A. 2013;19:75969. [PubMed: 23088577]

[46]. Feng P, Wei P, Shuai C, Peng S. Characterization of mechanical and biological properties of 3-D scaffolds reinforced with zinc oxide for bone tissue engineering. Plos One. 2014;9:e87755. [PubMed: 24498185]

[47]. Florczyk SJ, Wang K, Jana S, Wood DL, Sytsma SK, Sham J, et al. Porous chitosanhyaluronic acid scaffolds as a mimic of glioblastoma microenvironment ECM. Biomaterials. 2013;34:10143–50. [PubMed: 24075410]

[48]. Jana S, Florczyk SJ, Leung M, Zhang MQ. High-strength pristine porous chitosan scaffolds for tissue engineering. Journal of Materials Chemistry. 2012;22:6291–9.

[49]. Engler AJ, Sen S, Sweeney HL, Discher DE. Matrix elasticity directs stem cell lineage specification. Cell. 2006;126:677–89. [PubMed: 16923388]

[50]. Emmert M, Witzel P, Heinrich D. Challenges in tissue engineering - towards cell control inside artificial scaffolds. Soft Matter. 2016;12:4287–94. [PubMed: 27139622]

[51]. Benton JA, Kern HB, Anseth KS. Substrate Properties Influence Calcification in Valvular Interstitial Cell Culture. Journal of Heart Valve Disease. 2008;17:689–99. [PubMed: 19137803]

[52]. Dweck MR, Boon NA, Newby DE. Calcific aortic stenosis: a disease of the valve and the myocardium. J Am Coll Cardiol. 2012;60:1854–63. [PubMed: 23062541]

[53]. Duran E, Arriazu R. Quantification of Protein Expression on an Immunofluorescence Section by Using the MetaMorph Image Analysis System. Universal Journal of Applied Science. 2013;1:86–94.

[54]. Darby IA, Laverdet B, Bonté F, Desmoulière A. Fibroblasts and myofibroblasts in wound healing. Clin Cosmet Investig Dermatol. 2014;7:301–11.

Low magnification | High magnification

14%

16%

18%

50 μm | 10 μm
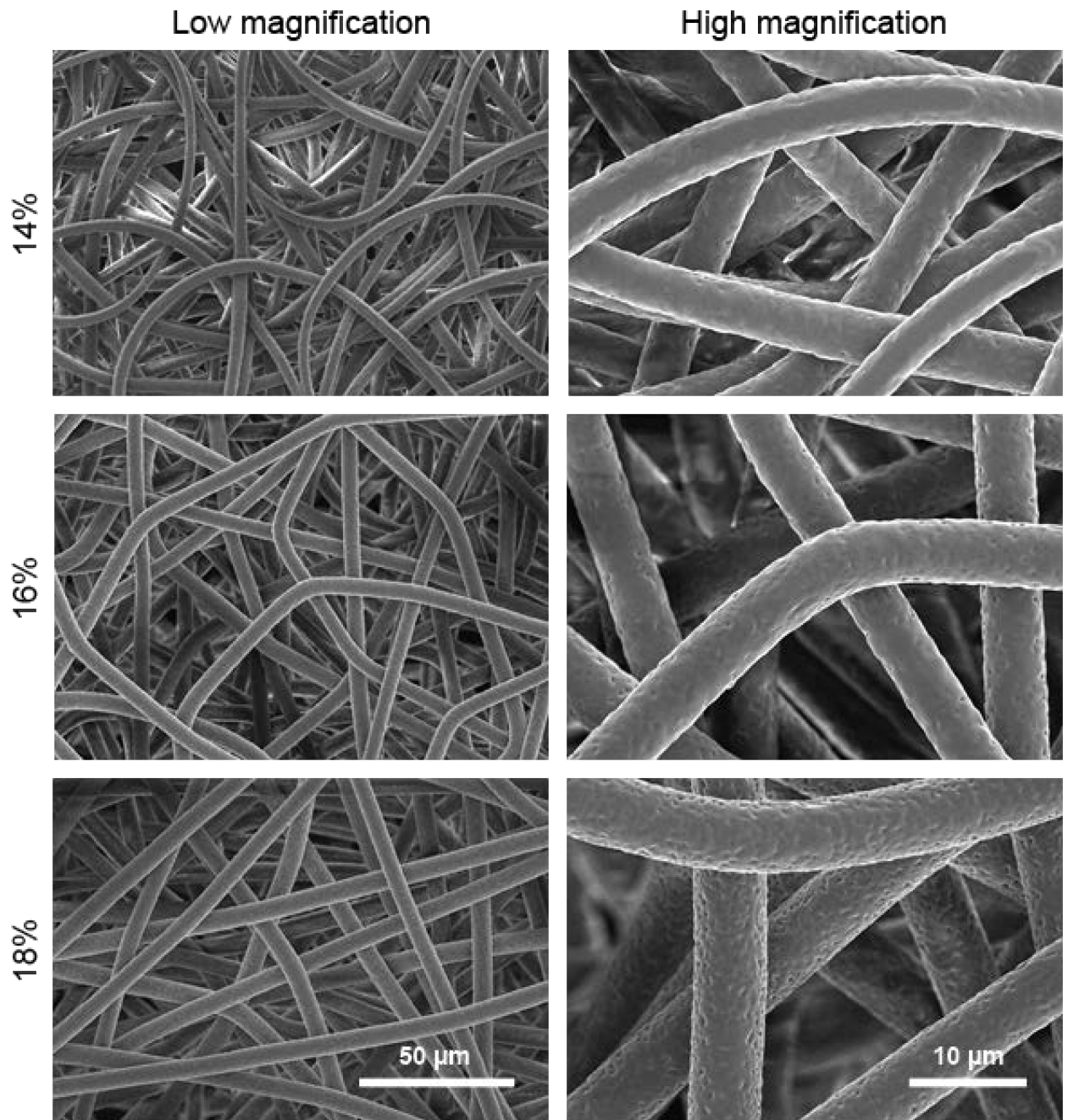
Figure 1:
Scanning electron microscopy (SEM) images of fibrous scaffolds produced by electro spinning 14%, 16% and 18% PCL solutions in chloroform solvent. Fibers in the scaffolds were uniformly distributed and fiber diameter in a scaffold was uniform.
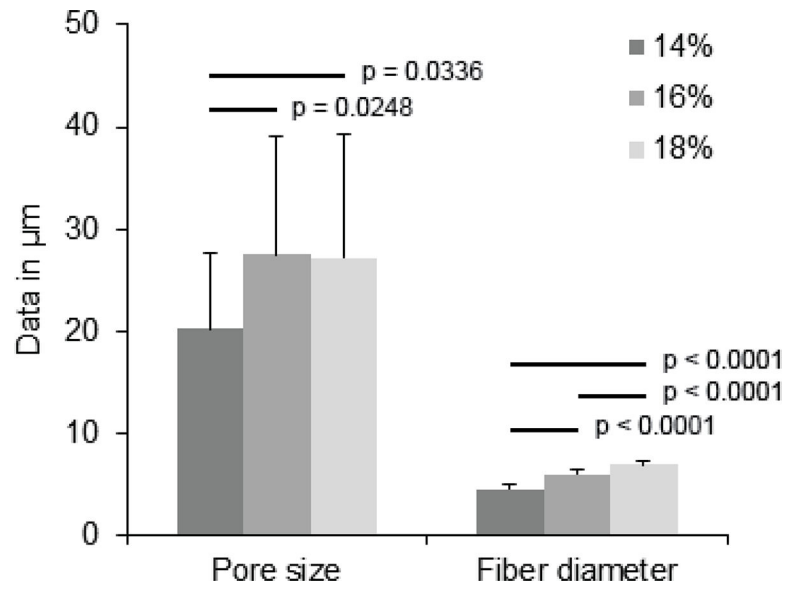
Figure 2:
Average pore size and fiber diameter were measured from SEM images of different types of scaffolds. Fiber diameters in the scaffolds were in micron scale and average pore size was sufficient for cell penetration into the scaffolds.
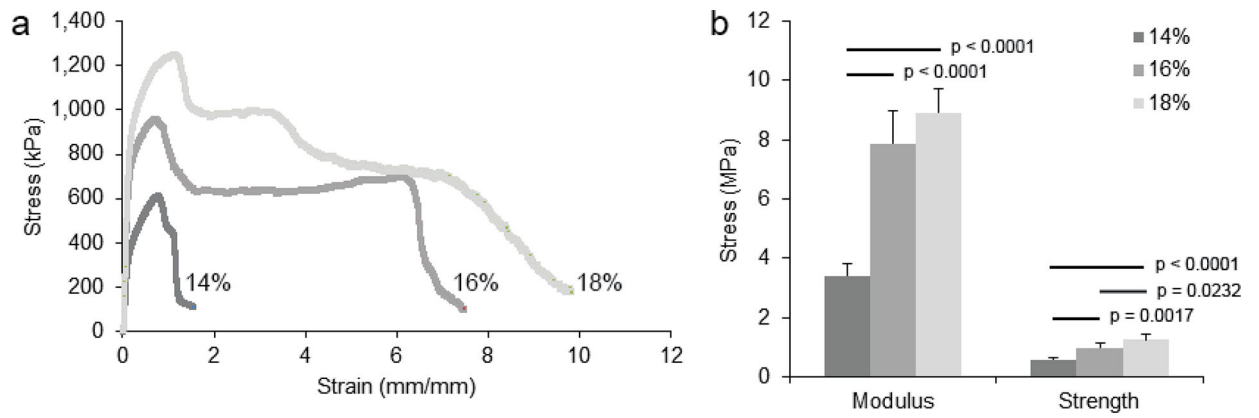
Figure 3:
Tensile properties of different types of scaffolds measured in a tensile tester. (a) Typical tensile curves of different types of scaffolds. (b) Tensile modulus and strength of each type of scaffold.
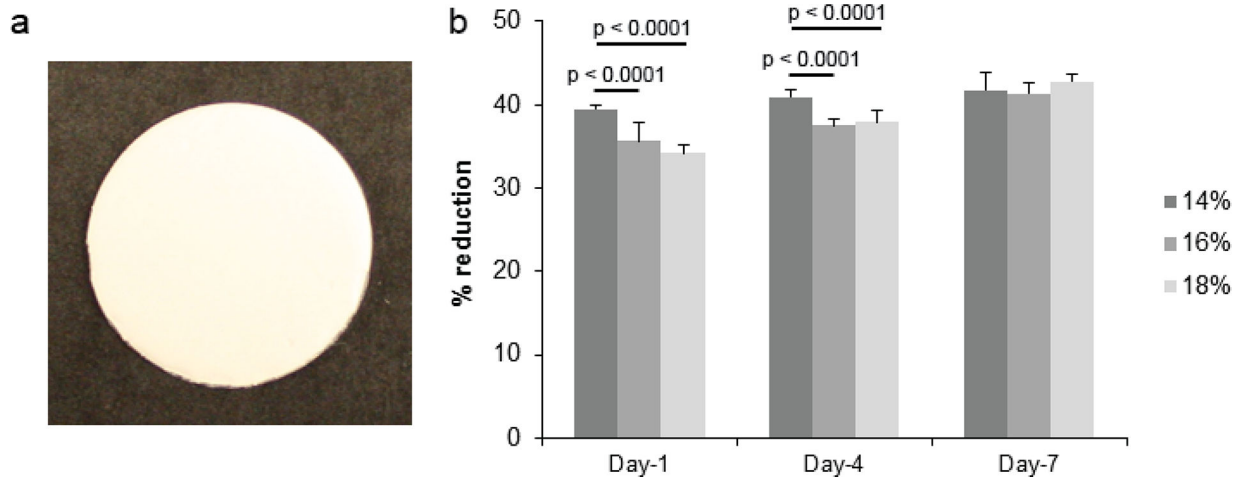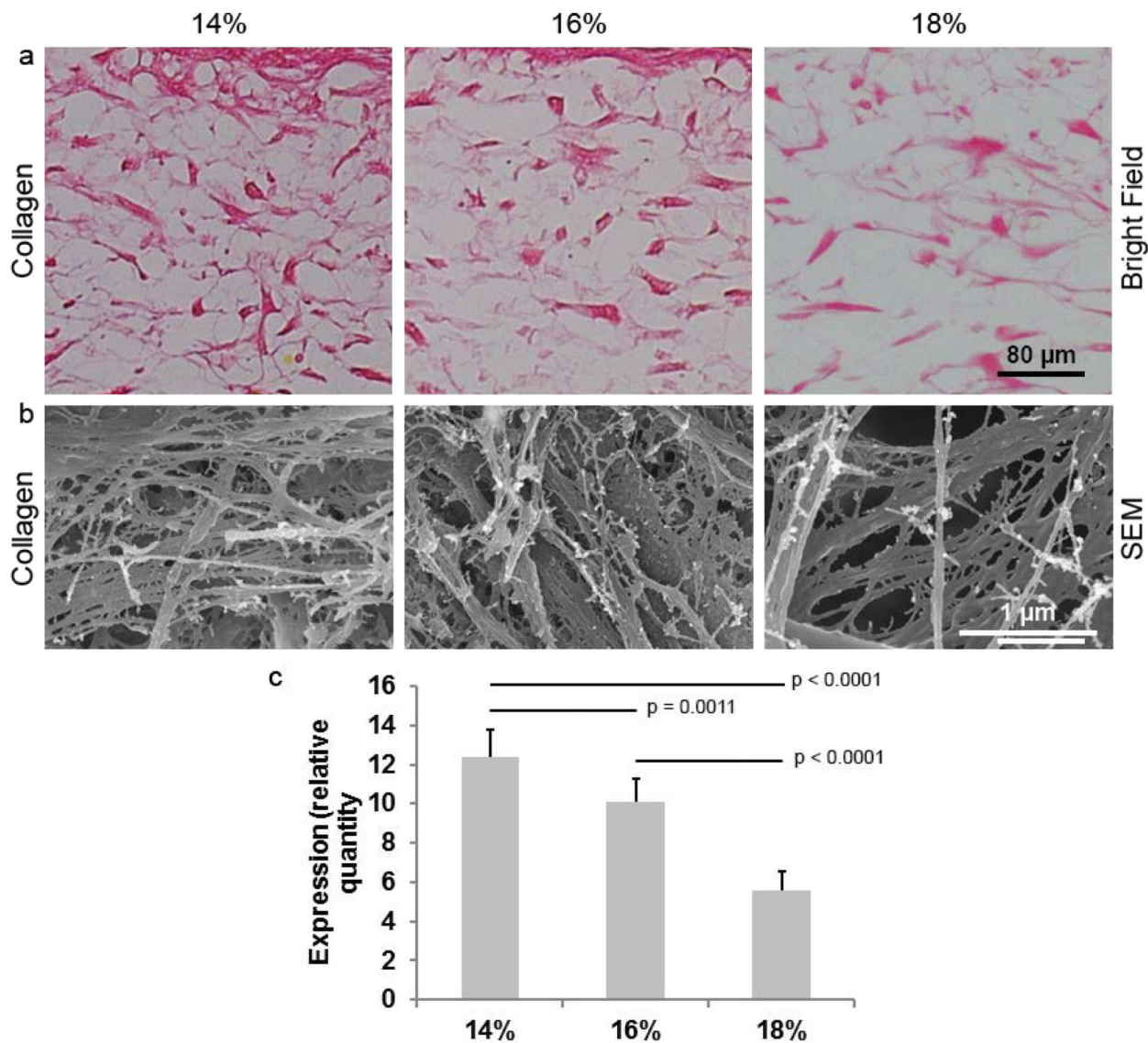
Figure 4:
Proliferation of porcine valvular interstitial cells (PVICs) on different types of scaffolds. (a) Circular-shaped scaffolds that fitted to wells of a 24-well plate were used for cell culture and for cell proliferation study. (b) Proliferation of PVICs on different types of scaffolds for 7-day time period in terms of percentages of Alamar Blue reductions.
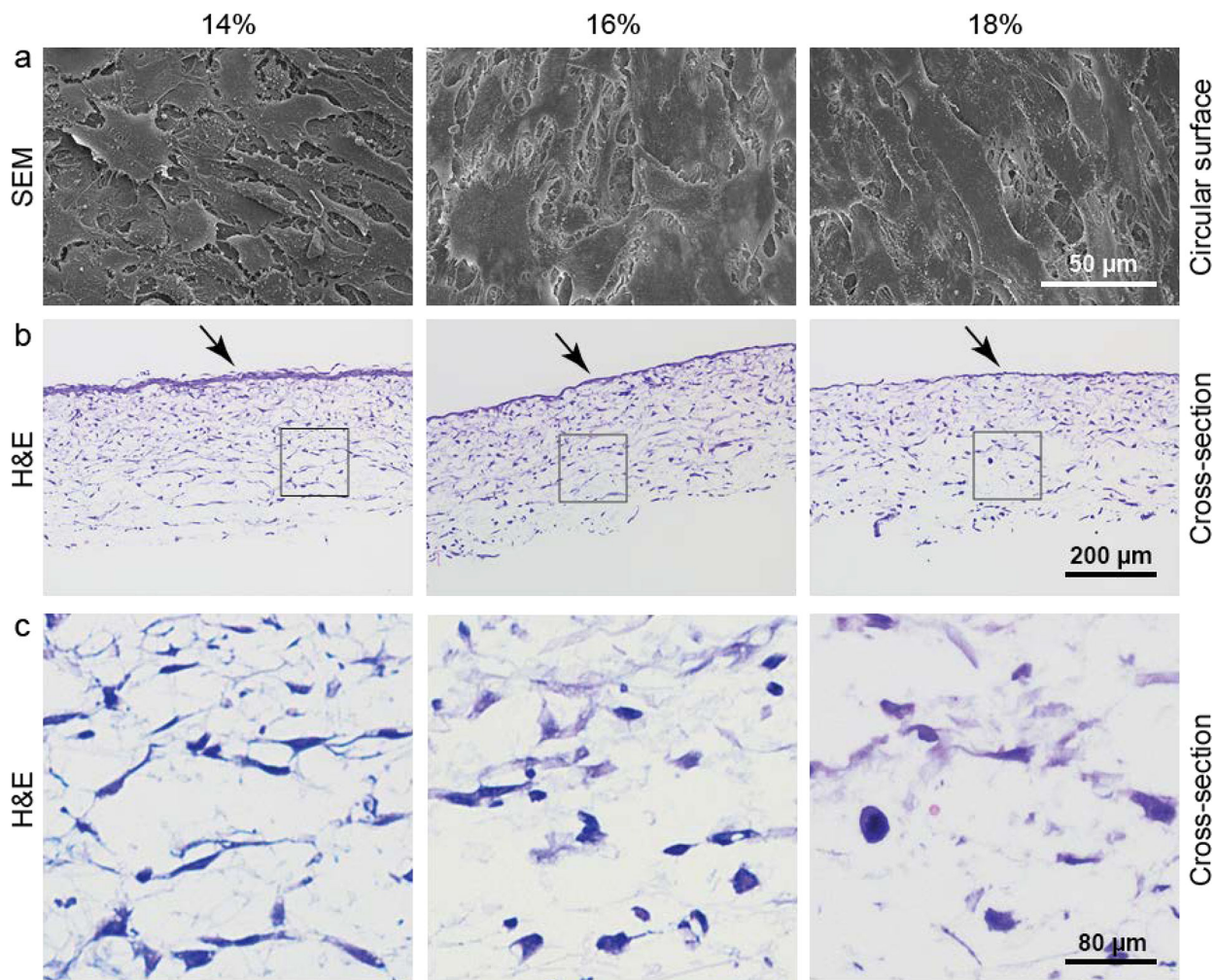
Figure 5:
Characterization of PVICs in 14%, 16% and 18% scaffolds after 14 days culture. (a) Morphologies of PVICs on the circular surfaces of these scaffolds obtained through SEM imaging. (b) Presence of PVICs inside these scaffolds was observed by H&E staining of the cross-sections of cultured scaffolds. A layer of cultured cells on the circular surface of the scaffold, is pointed by a black arrow. (c) At higher magnification, presence of PVICs in these scaffolds was distinct. Each image relates to the square section in the corresponding image in (b).
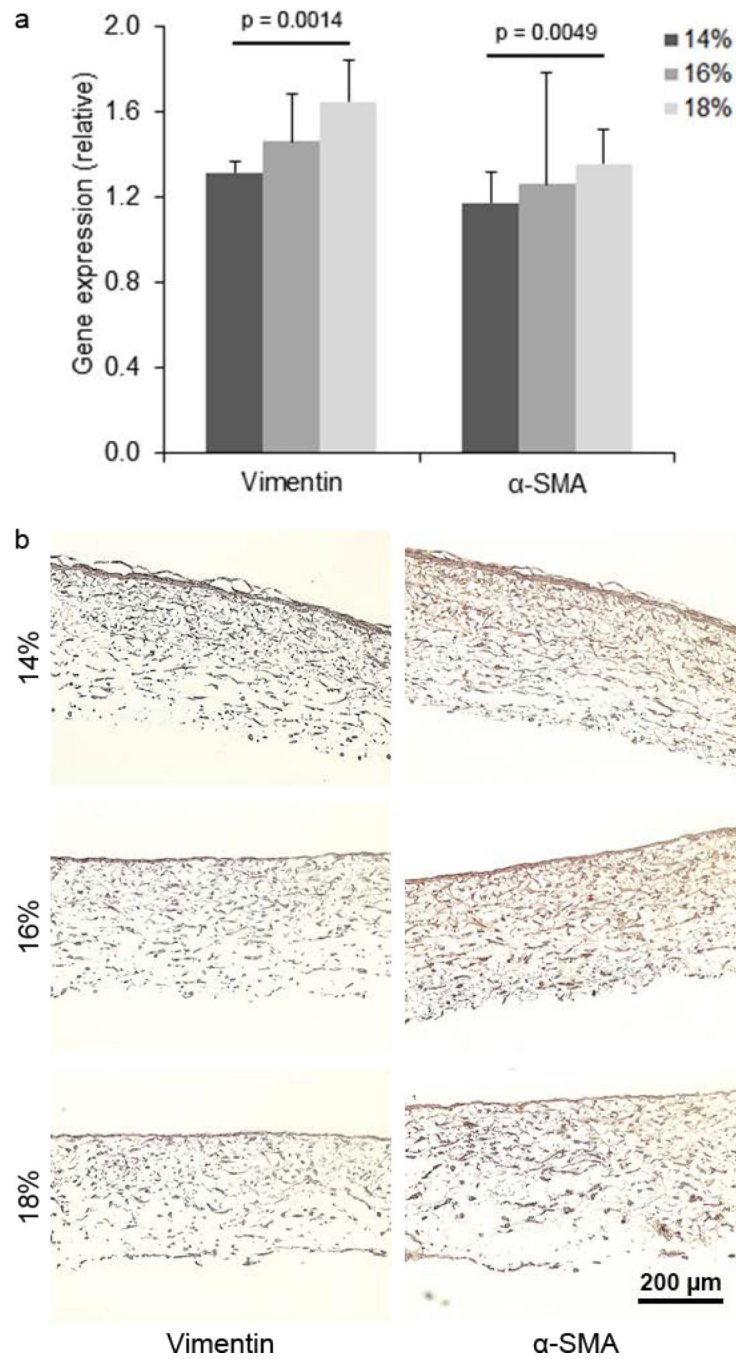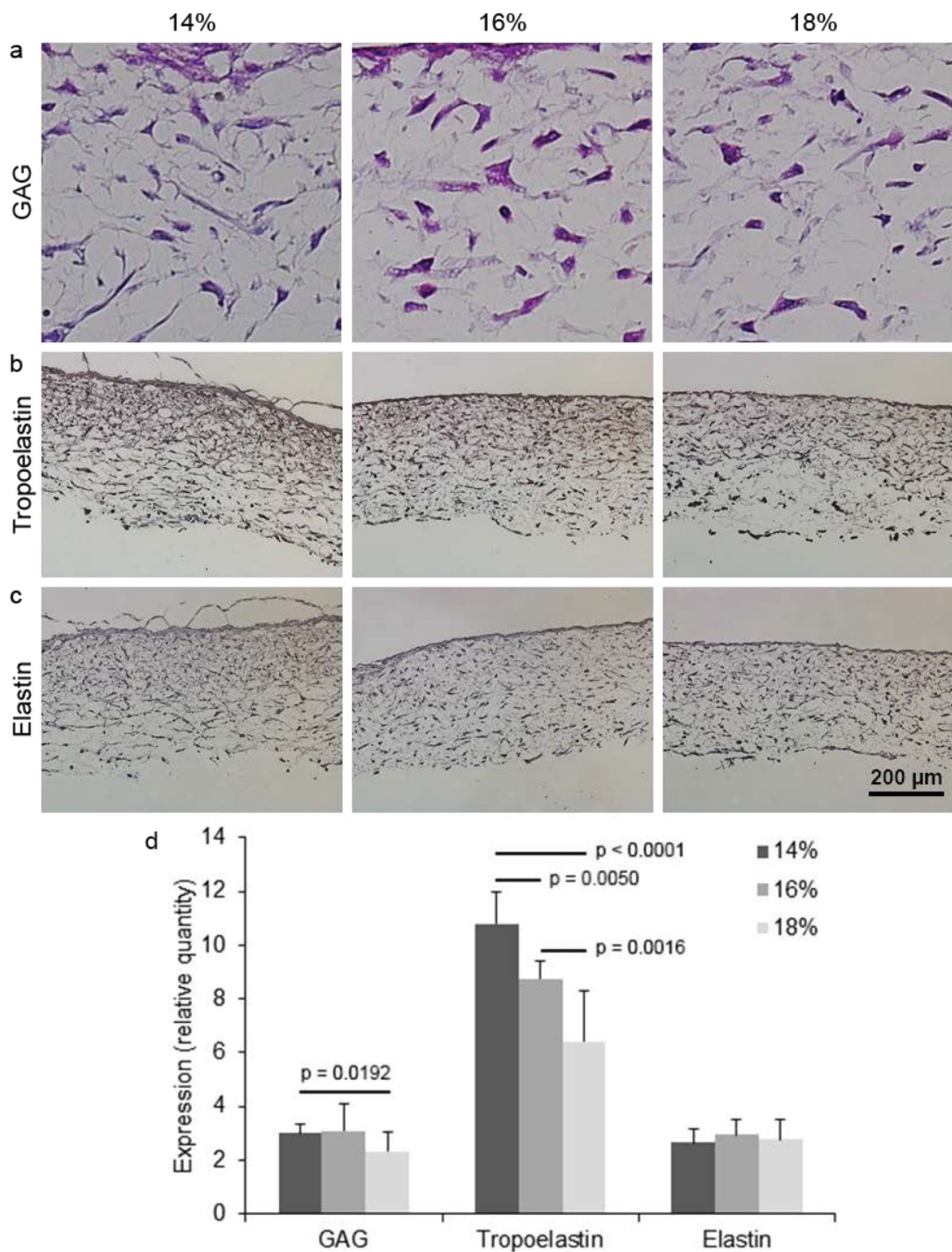
Figure 6:
Gene and protein expression of PVICs after 14 days of culture in different types of scaffolds, (a) Vimentin and α-smooth muscle actin (α-SMA) gene expression of PVICs were determined by RT-PCR. (b) Vimentin and α-smooth muscle actin (α-SMA) protein expression of PVICs were detected by immunohistochemical staining.
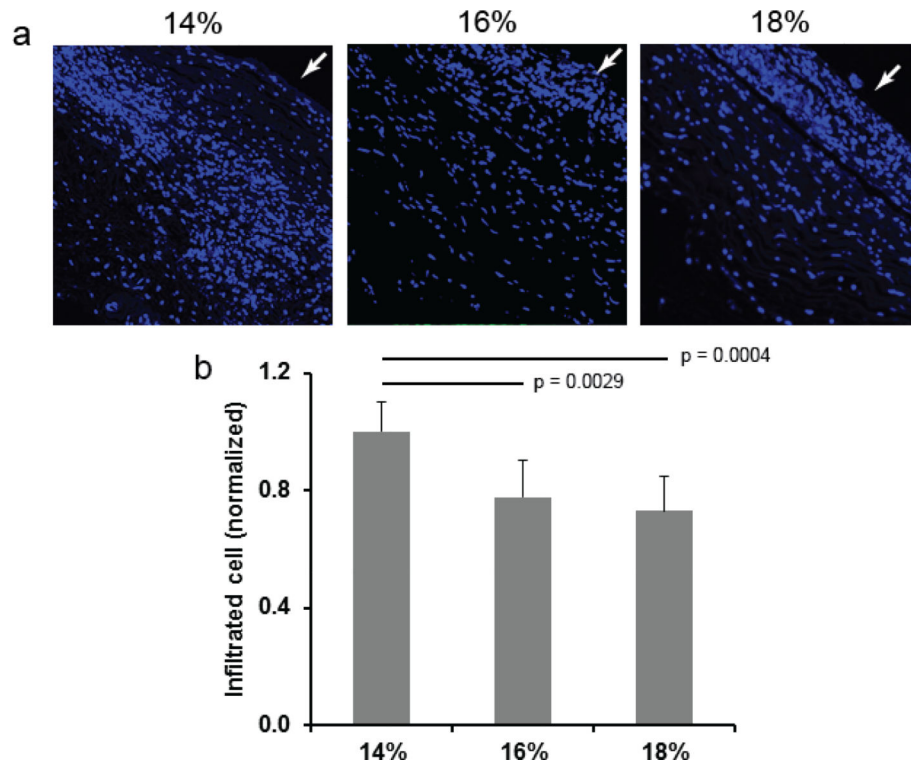
Figure 7:
Characterizations of collagen deposition by PVICs inside different types of scaffolds after 14 days culture. (a) Picrosirius red stained collagen was seen in all types of scaffolds in bright light. (b) The deposited collagen in all scaffolds was observed in their SEM images. (c) Graphical representation of quantified expression collagen protein in different types of scaffolds measured by a software-based method.
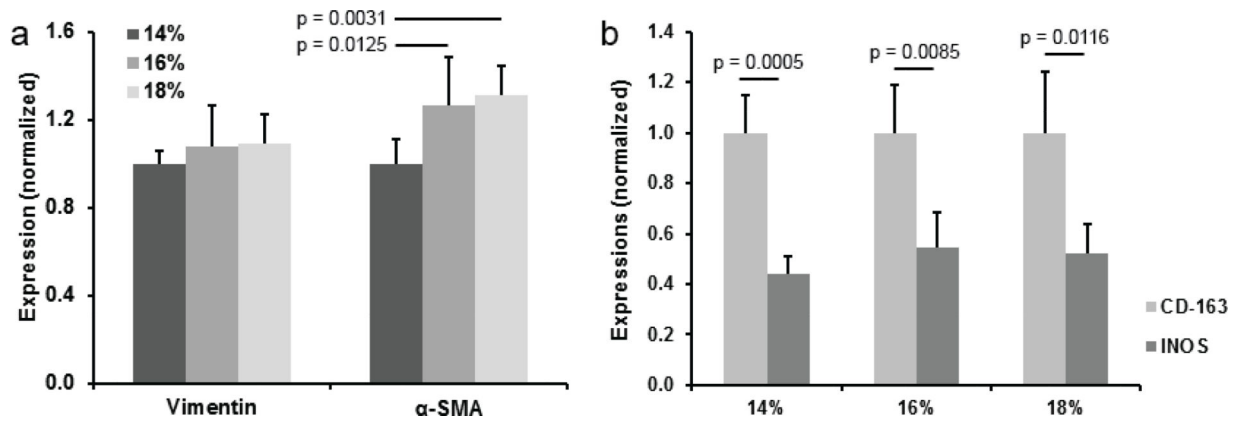
Figure 8:
Characterizations of deposition of other extracellular matrix including glycosaminoglycans (GAG), tropoelastin and elastin by PVICs in different types of scaffolds after 14 days culture. (a) Presence of Safranin O stained GAG deposited by PVICs was observed in different types of scaffolds, (b-c) Presence of immunohistochemical stained tropoelastin and elastin was observed in different types of scaffolds. (d) Graphical representation of quantified expression different ECM proteins in different types of scaffolds measured by a software-based method.

Figure 9:
Characterization of infiltrated cells in different types of scaffolds. (a) DAPI stained (nucleus staining) infiltrated cells in 14%, 16% and 18% scaffolds. White arrows show the scaffold surfaces attached to the skin of a rat during in vivo tissue engineering, (b) Graphical representation of quantified data of infiltrated cells in different types of scaffolds measured by a software-based method.

Figure 10:
Gene expression of infiltrated cells. (a) Vimentin and α-smooth muscle actin (α-SMA) gene expression of infiltrated cells, determined by RT-PCR. (b) CD-206 and INOS gene expression of infiltrated M2 and Ml phenotype macrophage cells, respectively, also determined by RT-PCR.